Eur. Phys. J. B **40**, 19–23 (2004)
DOI: 10.1140/epjb/e2004-00234-6

THE EUROPEAN PHYSICAL JOURNAL B

Low-height sputter-deposited magnesium oxide tunnel barriers: experimental report and free electron modeling

M. Hehn[1,a], C. de Buttet[1], G. Malinowski[1], E. Snoeck[2], C. Tiusan[1], and F. Montaigne[1]

[1] Laboratoire de Physique des Matériaux, UMR CNRS 7556, B.P. 239, 54506 Vandœuvre-les-Nancy Cedex, France
[2] CEMES-CNRS-Groupe NanoMatériaux, 29 rue Jeanne Marvig, B.P. 94347, 31055 Toulouse Cedex, France

Received 16 February 2004 / Received in final form 23 April 2004
Published online 3 August 2004 – © EDP Sciences, Società Italiana di Fisica, Springer-Verlag 2004

Abstract. Magnetic tunnel junctions with a barrier of magnesium oxide were prepared by plasma oxidation of sputter-deposited magnesium. They show magnetoresistance ratios up to 4.5% at room temperature and 5.5% at low temperatures for barrier thickness of 1.6 nm. The material exhibits low barrier heights of around 0.7 eV. These junctions follows the predictions of the free electron model which contrast with the predictions of band structure calculations and experimental results on epitaxial MgO based tunnel junctions.

PACS. 73.40.Rw Metal-insulator-metal structures – 75.70.Pa Giant magnetoresistance – 73.40.Gk Tunneling – 73.61.Ng Insulators

Large tunnel magnetoresistance (TMR) ratios are predicted from ab initio calculations in single crystalline Magnetic Tunnel Junctions (MTJ), namely Fe/MgO/Fe [1,2]. This motivated a significant experimental effort to grow such epitaxial stack using Molecular Beam Epitaxy with [3] and without [4] Mg post oxidation or using laser ablation [5]. As a result, 100% of TMR have been reported [6]. Far from the predicted 1000%, the 100% TMR signal is much larger than the one predicted by the Julliére's model [7]. Band structure effects have then to be invoked to explain this high TMR value but also features appearing in the variation of TMR with applied voltage [8].

As a reference, only few results are reported in literature on amorphous MgO tunnel barrier. With this material, tunneling has been shown using very thick MgO layers [9] (10 nm) but no results on thin and low resistance MgO barriers have been reported up to now. The scope of this paper consists to show that magnetoresistance ratios up to 5.5% can be achieved for MgO barrier thickness of 1.6 nm. The material exhibits low barrier heights of around 0.7 eV. These junctions follows the predictions of the free electron model which contrast with the predictions of band structure calculations: TMR increases with decreasing the barrier thickness. On this basis, high magnetoresistance ratios are forecast for junctions with very low resistance especially interesting for MRAM applications. Furthermore, for people working on epitaxial MgO based tunnel junctions, this paper contains datas that could answer their questions about the influence of the technological process on the junctions and especially on the junctions characteristics if barrier amorphization occurs.

Junctions are deposited onto float-glass substrates by sputtering tantalum, platinum, magnesium targets mounted on RF magnetron cathodes and cobalt on a DC magnetron cathode. The base pressure is less than 5×10^{-7} mbar and the substrates are maintained at room temperature. The studied samples are composed of Glass/Ta(5 nm)/Pt(20 nm)Co(10 nm)/MgOx(t_{Mg} nm, oxidized t_{Ox} s)/Co*(10 nm)/Pt(20 nm). All the layers are deposited at an operating pressure fixed to 5×10^{-3} mbar except the last Co layer of the stack, denoted by Co*, deposited at 1.5×10^{-2} mbar. In this way, two electrodes with different coercive fields could be made. To obtain the oxidized magnesium (MgO) barrier, the oxidation is realized just after deposition of the metallic Mg layer using a DC glow discharge at a power of 200 W and voltage 600 V under a pure 10^{-1} mbar O_2 plasma in the sputtering load-lock. The samples are transferred to this chamber without breaking the vacuum. The Mg nominal thickness t_{Mg} was varied from 1.6 nm to 3.5 nm and for each t_{Mg}, the oxidation time t_{Ox} has been optimized to get the highest TMR signal. As examples, t_{Ox} leading to the highest TMR signal is equal to 35 s when t_{Mg} equals 1.65 nm and 90 s when t_{Mg} equals 2.75 nm. In this letter, we report the results of the optimized junctions, the optimization will be published elsewhere [10].

[a] e-mail: hehn@lpm.u-nancy.fr

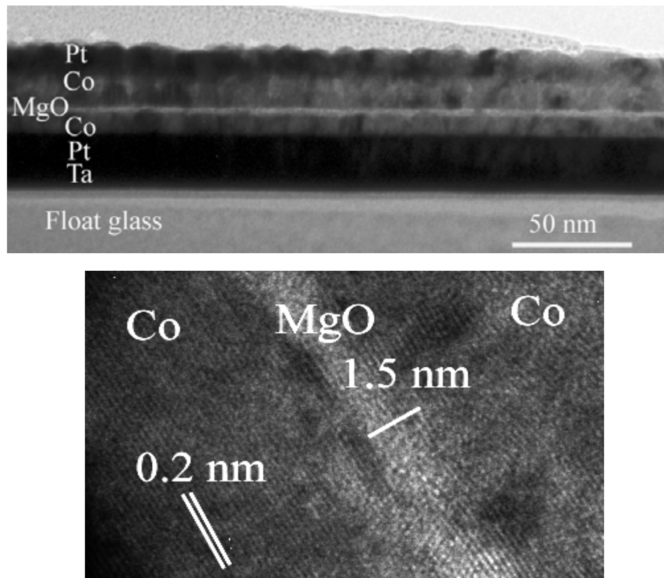

Fig. 1. Top: Low magnification TEM micrograph evidencing the continuity of the insulating barrier; bottom: HRTEM image evidencing the polycristallinity of the Pt, Co and MgO layers.

In a first step, the structural quality of the MgO tunnel barrier has been investigated at different scales using transmission electron microscopy and atomic force microscopy.

To study the structure and the microstructure of the stacking sequence, cross sectional samples for Transmission Electron Microscopy (TEM) experiments were prepared following the usual method. The TEM experiments were carried on a Philips CM30 microscope whose point resolution is 0.19 nm. Low magnification TEM images, as the one reported in Figure 1 (top), point out the continuity of the insulating barrier over at least a micron. The Co and Pt layers are polycrystalline with a typical grain size of about 10 nm. The interface roughness, the crystallinity and the thickness of the layers were studied in the High Resolution TEM (HRTEM) mode. The MgO barrier thickness is about 1.5 nm in accordance to the deposited layer thickness. In HRTEM micrograph in Figure 1 (bottom), lattice fringes appear in the Co (d_{hkl} = 0.2 nm) and Pt (d_{hkl} = 0.22 nm) layers corresponding to the {111} dense planes of the Co and Pt fcc structure. More surprisingly, considering the technique used to grow the MgO layer, lattice fringes appear also in the MgO oxide barrier with resolved d_{hkl} = 0.24 nm and d_{hkl} = 0.21 nm corresponding to the {111} and {100} planes of the NaCl type structure. Moreover, areas of the MgO barrier do not present those fringes. They correspond to locally amorphous material or to areas with crystallographic orientations not appropriated to resolve lattice fringes. Finally, from the structural point of view, the MgO layer is composed by a mixture of polycrystalline grains and amorphous material.

The roughness of the multilayer stack has been studied using atomic force microscopy (Fig. 2). First of all, roughness of the buffer bilayer Ta/Pt has been checked (Fig. 2a). Measured on a 1 μm square surface, the pic to

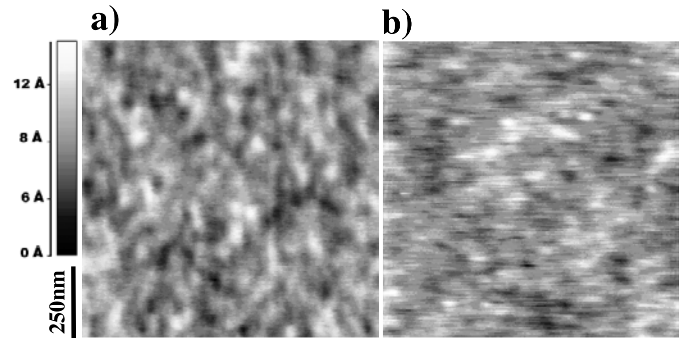

Fig. 2. Topography measured using atomic force microscopy on top of the buffer bilayer Ta/Pt (a) and on the top of the MgO barrier (b).

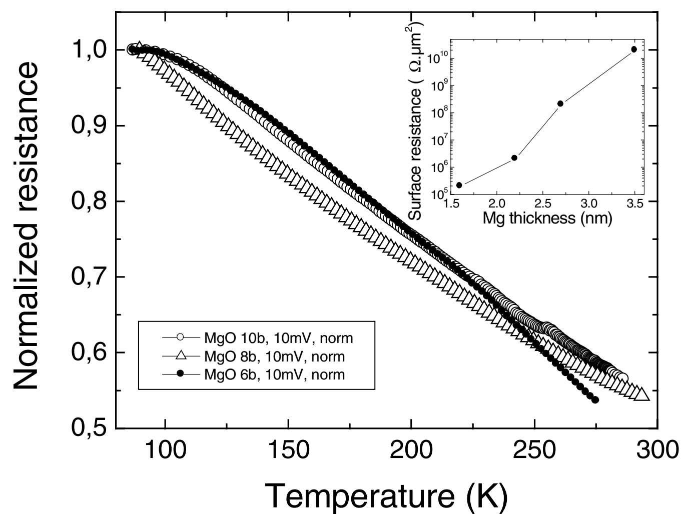

Fig. 3. Normalized Resistance to its higher value as a function of temperature measured at 10 mV for MgO tunnel junctions with deposited Mg thickness of 27.5 Å (-○-), 22 Å(-△-) and 16.5 Å (-●-). Inset: Variation of the tunnel junction sheet resistance as a function of deposited Mg thickness.

pic roughness, PP, is evaluated to 1.5 nm while the mean square root roughness, RMS, equals 0.19 nm. As far as the top MgO barrier roughness is concerned, both parameters are improved with PP equal to 0.97 nm and RMS equal to 0.12 nm.

To define the junction geometry for electronic transport measurements, we have used ex situ changed contact masks with a path width of 200 μm. Each sample was prepared to contain 14 tunnel junctions. Details on the junction geometry can be found elsewhere [11]. The electrical resistivity was measured with a standard four-probe DC technique. As shown by Akerman et al. [12] the most reliable tunneling criteria is the temperature-dependent conductivity. This last characteristic is reported in Figure 3 for an applied voltage of 10 mV and deposited Mg thickness of 27.5 Å (-○-), 22 Å (-△-) and 16.5 Å (-●-). No sign of electron hopping inside the barrier could be observed [13] and the mostly linear increase of resistance when temperature decreases is now currently admitted as a proof of a direct tunnel process through the barrier. The

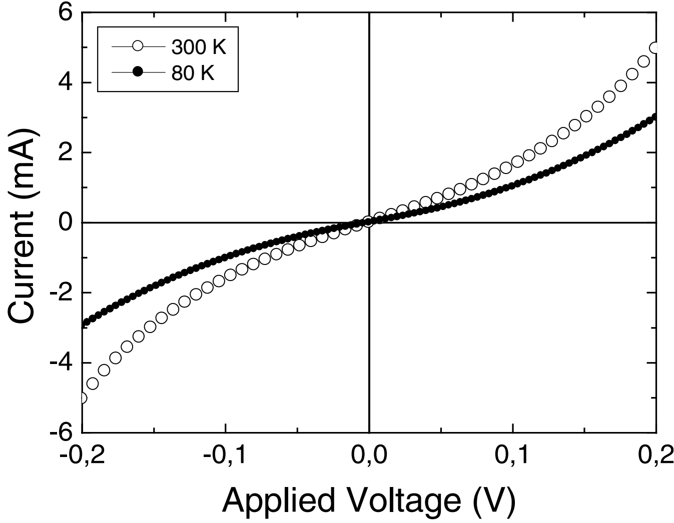

Fig. 4. Current/voltage characteristic measured at room temperature (-○-) and at 80 K (-●-) on a tunnel junction with 22 Å nominal Mg thickness.

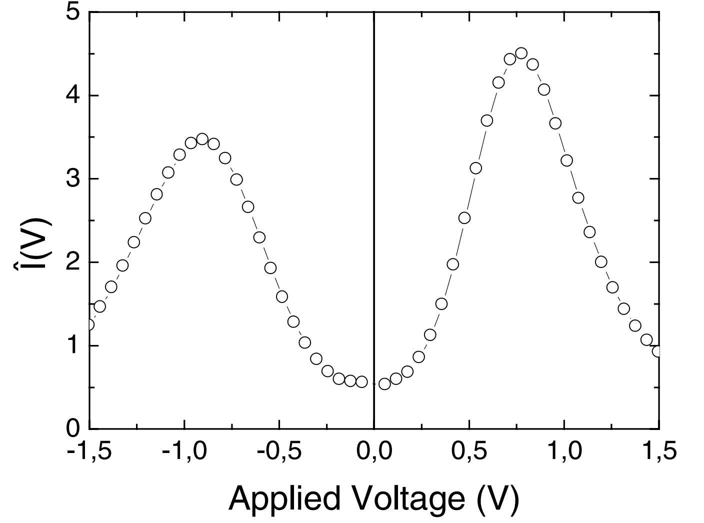

Fig. 5. $\hat{I}(V)$ curve measured on a Al_2O_3(0.7 nm)/MgO(1.6 nm) hybrid barrier. The MgO(1.6 nm)/Co interface barrier height was estimated, independently on the barrier thickness, to 0.75 eV.

50% of resistance increase when temperature decreases, larger than the 20% encountered using Al_2O_3 barriers, is a direct proof of the low tunnel barrier height and so a more pronounced effect of the smearing of the Fermi function as shown for example by Stratton [14]. As a consequence of electron tunneling, the surface resistance of the junction increases exponentially with the Mg nominal thickness as shown in the inset of Figure 3. The surface resistance of the junction, R_S, at 10 mV extends from 2×10^5 to 2×10^{10} $\Omega\mu$m^2. Considering the low barrier resistance of the 1.6 nm nominal thick Mg layer and the 4 points contact measurement technique, care has been taken to check the electrode resistance. Thanks to the use of Pt as electrode material, the square resistance of the electrode, $R_\square$, could be reduced down to $R_\square = 10\ \Omega$. The characteristic length above which current distribution effects appear for the lowest resistance junction is [15]

$$\lambda = \sqrt{\frac{R_S}{R_\square}} = 150\ \mu\text{m}. \tag{1}$$

Considering the 200 μm lateral size of our tunnel junction, the results of the 1.6 nm nominal thick Mg oxidized tunnel barrier are not affected by current distribution effects. However, even if no technical growth limitations were met, it is not possible to further reduce the thickness of the tunnel barrier without geometric effects in 200 μm lateral size junction. Work is under way to reduce both the Mg thickness and the junction lateral size by using lithography patterning.

For all junctions on a sample, the current/voltage characteristics ($I-V$ curves) were determined. The samples showed an average yield of about 90% and, as a corollary of electron tunneling, a typical symmetric non linear tunnel-like $I-V$ curves (Fig. 4). Barrier heights and thickness were determined using the Brinkman formula [16]. The barrier height was estimated to 0.7 eV and the barrier thickness was estimated to approximately the Mg nominal thickness. Somewhat surprising, plotting the normalized temperature dependence $\hat{I}(V) = [I(V,T)-I(V,0)]/I(V,0)$ as a function of V does not produce cusps at voltages corresponding to the barrier height [17]. This is due to the appearance of current distribution effects when the applied voltage is above 0.5 V. Indeed, for strong applied voltages, R_S decreases and λ becomes smaller than the lateral size of the junction. One way to circumvent this limitation consists to grow Glass/Ta/Pt/Co/Al_2O_3/MgO/Co/Pt hybrid tunnel barriers. Adding Al_2O_3 to the barrier increases the resistance of the junction and current distribution effects disappear even at high applied voltages. So, in the $\hat{I}(V)$ curve, barrier height of the Co/Al_2O_3 and MgO/Co interfaces can be measured. An example is given in Figure 5 for a Al_2O_3(0.7 nm)/MgO(1.6 nm) hybrid barrier. Here again, the MgO barrier height was estimated, independently on the barrier thickness, to 0.75 eV. A full analysis of hybrid Al_2O_3/MgO tunnel barriers will be published separately [18]. Finally, a last method has been used to get an estimation of the MgO barrier height. According to the inset of Figure 3, the MgO surface resistance increases exponentially with the Mg nominal thickness. This variation has been theoretically predicted using the following equation

$$\ln(R_S) = Ad\sqrt{m^*\Phi} + B \tag{2}$$

where Φ is the barrier height, d the barrier thickness, m^* is the effective mass inside the barrier, A and B are constants. A fit of $\ln(R_S)$ versus d leads to $m^*\Phi =$ 0.5 eV. Considering $m^* = 1$, this last set of measurements confirms the low barrier height of the sputtered MgO material.

The magnetoresistance ratio has been measured on resistance versus applied field curves (inset Fig. 6) and has been studied as a function of applied voltage, TMR(V).

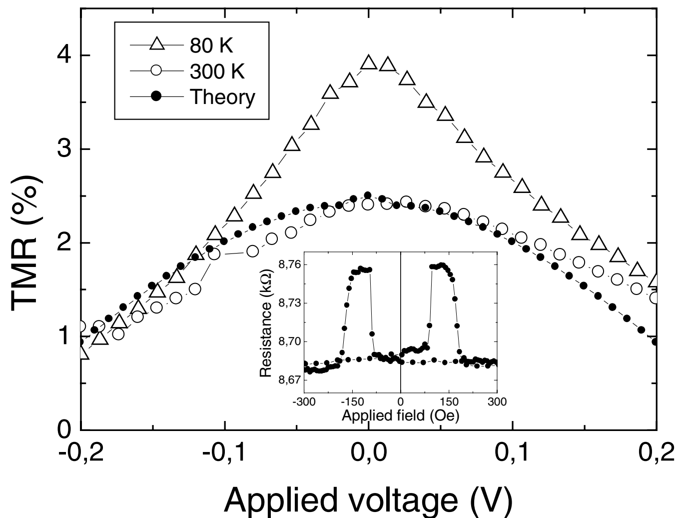

Fig. 6. Voltage dependence of the magnetoresistance ratio measured at room temperature (-○-) and at 80 K (-△-) on a tunnel junction with 22 Å nominal Mg thickness. Theoretical voltage dependence of the magnetoresistance ratio computed using the free electron model for a 20 Å MgO thickness (-•-). Inset: resistance versus applied field measured on a 2.75 nm thick MgO barrier at 10 mV.

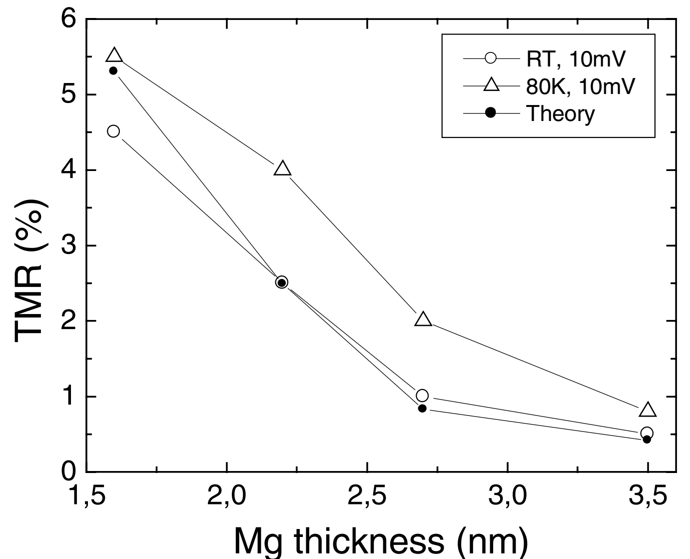

Fig. 7. Variation of the magnetoresistance ratio with the nominal Mg thickness measured at room temperature (-○-) and at 80 K (-△-). Theoretical magnetoresistance ratio dependence with the MgO thickness computed using the free electron model for a 0.7 eV barrier height (-•-).

An example is given in Figure 6 for the 2.2 nm thick nominal Mg tunnel barrier. The magnetoresistance ratio is reduced to half of its maximum value at bias voltages $V_{1/2}$ of about 0.2 V. This value is smaller than the one corresponding to Al_2O_3 barriers and it represents another indication of the low barrier height of magnesium oxide, as also observed with tantalum oxide [19] and explained with the free electron model (FEM) developed previously [20]. The parameters extracted from the Brinkman fit at room temperature have been injected in the FEM and the experimental TMR(V) curve (Fig. 6, (-○-)) could be well reproduced theoretically using an unit effective mass inside the barrier (Fig. 6, (-•-)). Finally, TMR has been studied as a function of Mg nominal thickness. As can be seen in Figure 7, a strong increase of the TMR signal is observed when Mg thickness is decreased. Here again, the experimental curve (Fig. 7, (-○-)) could be well reproduced theoretically (Fig. 7, (-•-)) using a barrier height of 0.7 eV, a unit effective mass and the free electron model. This definitely shows that sputter-deposited MgO barriers, composed by polycrystalline and amorphous regions, follow the FEM predictions and that no band structure effects are evidenced. Then, spin filtering by the tunnel barrier and symmetry filtering by the couple (ferromagnetic electrode/tunnel barrier) require epitaxial magnetic tunnel junctions. As soon as a polycrystalline and/or an amorphous barrier is grown, band effects are smeared out and the FEM applies with effective barrier height and thickness. These parameters are the result of an average over the tunnel junction surface of the wave vector dependent tunnel probabilities.

To summarize, magnetic tunnel junctions made with a post oxidation of a sputter-deposited Mg layer have been successfully grown. They have been shown to follow the prediction of the FEM: variation of TMR(V), variation of resistance and TMR with barrier thickness. Limited by the current distribution with the actual size of the junction, a magnetoresistance ratio of 5.5% could be reached experimentally and confirmed theoretically with a 1.6 nm nominal thick Mg layer. The development of the lithography process is under way to reduce the junction size down to 1 μm that will us allow to study junctions with thickness down to 1 nm without current distribution effects. Potentially with this barrier thickness, a TMR ratio of 15% is forecasted within the free electron model. With a low barrier height of 0.7 eV, a low surface resistance and a TMR of 15%, the material appears interesting for applications like magnetic access memories. From the fundamental point of view, inducing texture in the MgO barrier by post annealing is the key to converge towards the behavior highlighted in epitaxial MgO tunnel barriers. This work is underway.

The author would like to thank D. Lacour and A. Schuhl for valuable discussions. This work is partially supported by 'La Région Lorraine'.

References

1. J. Mathon, A. Umerski, Phys. Rev. B **63**, 220403R (2001)
2. W.H. Butler, X.-G. Zhang, T.C. Schulthess, J.M. MacLaren, Phys. Rev. B **63**, 054416 (2001)
3. S. Mitani, T. Moriyama, K. Takanashi, J. Appl. Phys. **93**, 8041 (2003)
4. E. Popova, J. Faure-Vincent, C. Tiusan, C. Bellouard, H. Fischer, M. Hehn, F. Montaigne, M. Alnot, S. Andrieu, A. Schuhl, Appl. Phys. Lett. **81**, 1035 (2002)

5. M. Bowen et al., Appl. Phys. Lett. **79**, 1655 (2001)
6. J. Faure-Vincent, C. Tiusan, E. Jouguelet, F. Canet, M. Sajieddine, C. Bellouard, E. Popova, M. Hehn, F. Montaigne, A. Schuhl, Appl. Phys. Lett. **82**, 4507 (2003)
7. M. Julliére, Phys. Lett. A **54**, 225 (1975)
8. C. Tiusan et al., submitted to Phys. Rev. Lett. (2003)
9. C.L. Platt, B. Dieny, A.E. Berkowitz, J. Appl. Phys. **81**, 5523 (1997)
10. M. Hehn, in preparation for J. Appl. Phys. (2003)
11. M. Hehn, O. Lenoble, D. lacour, C. Féry, M. Piecuch, C. Tiusan, K. Ounadjela, Phys. Rev. B **61**, 11643 (2000)
12. J.J. Akerman, R. Escudero, C. Leighton, S. Kim, D.A. Rabson, R.W. Dave, J.M. Slaughter, I.K. Schuller, J. Magn. Magn. Mat. **204**, 86 (2002)
13. Y. Xu, D. Ephron, M.R. Beasley, Phys. Rev. B **52**, 2843 (1995)
14. R. Stratton, Phys. Chem. Solids **23**, 1177 (1962)
15. F. Montaigne, F. Nguyen Van Dau, A. Schuhl, J. Magn. Magn. Mat. **217**, 231 (2000)
16. W.F. Brinkman, R.C. Dynes, J.M. Rowell, J. Appl. Phys. **41**, 1915 (1970)
17. P. Rottländer, M. Hehn, A. Schuhl, Phys. Rev. B. **65**, 054422 (2002)
18. C. de Buttet et al., in preparation (2004)
19. P. Rottländer, M. Hehn, O. Lenoble, A. Schuhl, Appl. Phys. Lett. **78**, 3274 (2001)
20. F. Montaigne, M. Hehn, A. Schuhl, Phys. Rev. B. **64**, 144402 (2001)